Geopersia ***9*** *(2), 2019, PP. 279-292* *DOI: 10.22059/GEOPE.2019.264206.648410*

Analysis of fold and fault-related fracture systems development using image logs at Asmari Formation in the Rag Sefid Anticline, SW Iran

Mehdi Yousefi *, Seyed Morteza Moussavi, Mohammad Mehdi Khatib
Department of Geology, Faculty of science, University of Birjand, Birjand, Iran
**Corresponding author, e–mail: geomehdi66@birjand.ac.ir*
(*received: 21/08/2018 ; accepted: 03/02/2019*)

Abstract

Image logs of 13 wells in the Rag Sefid Anticline show two systems of fractures developed under two deformation phase in the Dezful Embayment. This deformation phases are folding resulted from Zagros NE contraction and reactivation of the basement fault rotated the fold axial trace within the Hendijan-Izeh fault zone. Folding phase comprises four sets of fractures, which include axial and cross axial sets that trend parallel and perpendicular to the fold axial trace, respectively and two oblique sets that trend at moderate angles to the axial trace in the eastern part of the fold. Reactivation of the Hendijan-Izeh Fault has caused the restraining bend and dextral shear zone in the western part of the Rag Sefid Anticline. This dextral shear has produced three fracture sets which include two sets of Riedel shear fractures and an extensional set. The mean shortening directions measured from the fold and fault related fracture systems in the eastern and western parts of Rag Sefid Anticline are N022±2° and N064±1°, respectively. The measured NNE and ENE shortening orientations in the well sites is consistent with maximum horizontal stress orientations derived from earthquake focal mechanism solutions and with the absolute plate motion direction of the Arabian Plate with respect to Eurasia in the Dezful Embayment.

Keywords: *Asmari Formation, Rag Sefid Anticline, Fracture Systems, Hendijan-Izeh Fault, Image logs.*

Introduction

A number of regional studies have demonstrated the compressional reactivation of preexisting structures within both the cover and the basement of foreland thrust belts worldwide (e.g., Alps: Lacombe & Mouthereau, 2002; Taiwan: Mouthereau *et al*., 2002). Moreover, reactivation of the intraplate basement faults and structural inversion of sedimentary basins have been documented in the foreland far from the orogens (e.g., Tapponnier *et al.,* 1986; Ziegler *et al.,* 1995; Lacombe & Mouthereau, 1999; Marshak *et al.,* 2000). The development of various trends of fracture is affected by reactivation of the faults. The understanding of the factors controlling the fracture patterns such as orientation, distribution, density, spatial variation and chronology is important to improve the methods used in the fractured reservoirs. Furthermore, from a regional-scale point of view, this understanding is of major interest for development plans of these reservoirs, which can constitute petroleum provinces like the Southwest Zagros Mountains (Ahmadhadi *et al.,* 2008). The high productivity of the Zagros Mountains reservoirs is related to the presence of two systems of fractures that have led to secondary effective porosity in the carbonate reservoirs (Ahmadhadi *et al.,* 2008). In the Southwest Zagros Mountains Several sets of fold-related fractures, which constitute the first system, have well defined relationships to the fold structural elements and occur within the boundaries of the fold structures. The spatial variation of these sets of fractures is a function of the spatial variation of the fold elements and also position within the fold-thrust belt. Many studies have tried to relate development of micro and meso-structural pattern of fractures respect to fold geometrical elements, such as fold axis, forelimb, back limb and termination (Gholipour, 1998; Wennberg *et al.,* 2006; Inigo *et al.,* 2012). The second fracture system includes several sets of basement faults, and their related, subsidiary fractures, that cut through the folded Phanerozoic sedimentary sequence in the Zagros Fold and Thrust Belt (ZFTB). While the spatial density and variation of the fold-related fractures correlate with folds themselves, the fault-related fracture system is localized along isolated linear zones, possibly marking the boundaries of basement blocks (Mobasher & Babaie, 2008). Because of the essential role of fractures in the hydrocarbon production from the Dezful Embayment (Southwest Zagros Mountains) oil fields, many studies have been done in this area to describe the fracture population within carbonate reservoirs. Among the studied formations, the Asmari Formation is famous with regards to fracture studies because (i) this Oligo-Miocene formation crops out in a 1200 km

long by 200 km wide belt expanding from the northeast Iraq to the southwest Iran. (ii) It also includes most of the hydrocarbon reservoirs in this part of the ZFTB (e.g., Beydoun, 1992). The orientation of open fractures relative to the anticline axis, or relative to the Hendijan Fault trend, is the most important reason for the separation of the fold-related fracture and the fault related fractures. Therefore we have applied FMI and FMS resistivity image logs of 13 developmental wells in the Rag Sefid Anticline to help establish the kinematic relationships of the fold and fault structures and analyze the tectonic history of the South Dezful Embayment. The main purposes of this research include: (i) identifying and distinguishing between fold and fault related fracture sets, (ii) determining the kinematic importance of each fracture system and (iii) comparing the direction of shortening resulted from analysis of each system and applying the knowledge of the spatial variation in the orientation of the kinematic axes to the understanding of Zagros orogenic movements.

Geological Setting

The Zagros fold and thrust belt (ZFTB) trending NW-SE to nearly E-W is resulted from several deformation events from Late Cretaceous (Vernant *et al.,* 2004) (Fig. 1 a). This fold and thrust belt is currently undergoing 20–25 mm/yr shortening (Vernant *et al.,* 2004) and thickening as a result of collision of the Arabian and Central Iran plates (Berberian, 1995). This folded belt provides a good example of convergence partitioning in its NW part, the overall NW-SE convergence between the Arabian and Eurasian plates being accommodated by dextral strike-slip movement at the rear of the belt along the Main Recent Fault (Talebian & Jackson, 2002) and by belt-perpendicular shortening leading to the formation of N140 trending folds (Hessami *et al.,* 2001; Agard *et al.,* 2005). The Zagros folded belt has been divided into several morphotectonic regions. These main morphotectonic regions are limited by deep seated basement faults (Fig. 1). Two major tectonic trends, respectively N-S and NW-SE, are known in the Arabian Shield and there is evidence for the continuation of these trends northward into the Zagros orogenic belt (Bahroudi *et al.,* 2003). In the Zagros belt, the approximate locations and geometries of the basement faults have been defined using geodetic survey, more or less precise epicenter/hypocenter locations, as well as topographic and morphotectonic analyses. The first group of basement faults includes the Mountain Front Fault (MFF), the Dezful Embayment Fault (DEF), and the Zagros Foredeep Fault (ZFF).

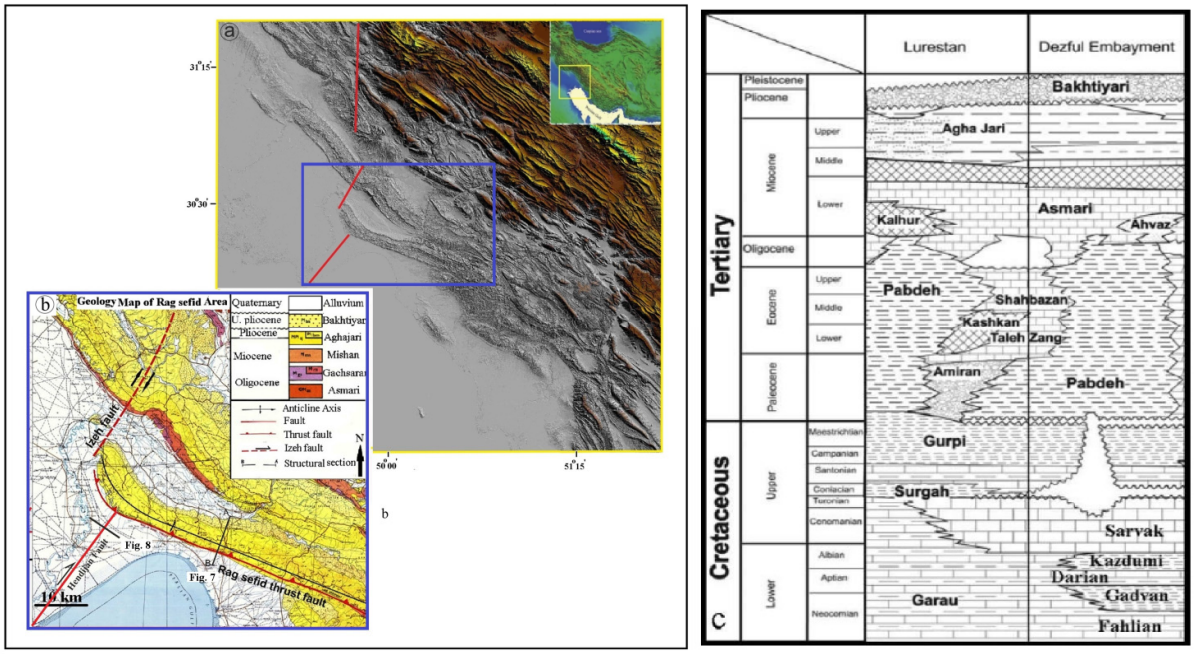

Figure 1. a Location of the Rag sefid Anticline in the Zagros folded belt. b Geological map of the Rag sefid Anticline. c Lithostratigraphy chart in the studied area since Lower Cretaceous.

Fault plane solutions for earthquakes along these faults indicate that they all dip about 60^{O} NE, suggesting that they now act as reverse faults although they may have acted as normal faults during the Permo-Triassic opening of the Neo Tethys ocean (Berberian, 1995). Another group of basement faults are N-S trending faults which developed during the latest Proterozoic and Early Cambrian in the Arabian basement (Beydoun, 1992). During the Triassic and Late Cretaceous, N-S trending uplifted zones and basins were related to the intermittent reactivation of this group of basement faults (Sherkati & Letouzey, 2004). These faults are steeply dipping and currently undergo right-lateral strike-slip motion (Berberian, 1995; Hessami *et al.,* 2001). As presented in Fig. 1.b, some of these faults located in the Zagros belt, are the Hendijan- Izeh Fault (HIF), the Kharg-Mish Fault (KMF) and the Kazerun Fault (KZ). Structural information resulted from seismicity within the Zagros belt proves that these faults are still active as right lateral strike-slip faults in the basement underlying the folded cover (Jackson & McKenzie, 1984; Berberian, 1995; Talebian & Jackson, 2002). The study area is located in southern west margin of the Dezful Embayment. The Dezful Embayment corresponds to a morphotectonic region stepped down with respect to the Izeh Zone, surrounded by three of the major basement structures described above. The northwestern border is the Balaroud Flexure, the east-northeastern border is the Mountain Front Fault (MFF) and its south-southeastern border is the Kazerun Fault (Sepehr & Cosgrove, 2004). As presented in Fig. 1.c, generally three main lithological series are exposed in this area from Lower Cretaceous up to Pliocene; (i) Carbonate series, including part of the Khami Group (Fahliyan and Dariyan Formations, of Neocomian and Aptian age, respectively), Ilam and Sarvak Formations (Cenomanian to Santonian) and the Asmari Formation (Oligocene-Lower Miocene); they form the main reservoir rocks in southwest Iran. (ii) Clastic and argillaceous series, including the Gadvan Formation of the Khami Group (Neocomian-Aptian), Kazhdumi (Albian), Gurpi (Campanian- Maastrichtian), Pabdeh (Paleocene-Eocene), Mishan, Agha-Jari and Bakhtiary formations (Upper Miocene-Lower Pleistocene). The Kazhdumi and Pabdeh formations are well known as petroleum source rocks in the region. (iii) Evaporitic series, including the Kalhur Member (Lower Miocene) within the Asmari Formation and the Gachsaran Formation (Middle Miocene), which is the main cap rock of the Asmari reservoirs in Iran. The Rag sefid Anticline is located in the south of the Dezful Embayment, close to the Hendijan-Izeh Fault, one of the major NNE– SSW trending right-lateral strike-slip fault systems in the Zagros Simply Folded belt. The Rag Sefid structure is boomerang shape and is surrounded by other adjacent structures such as Bibi-Hakimeh, Pazanan, Agha-Jari, Ramshir, Tangu, Zageh and Hendijan. The overall axial trend is about WNW–ESE; however, the western part of this anticline has NNW–SSE trend. This fold is asymmetric and characterized by a high angle southwestern forelimb due to faults development in this limb. This structure has 54 Km length and 4-8 Km width located between 29° 50′ N and 30° 35′ N latitudes, and between 49° 42′ E and 50° 054′ E longitudes. This anticline has three reservoir horizons, are the Khami Group (Gas bearing), Bangestan Group and Asmari Formation (Oil/Gas bearing). Based on biostratigraphical data, there is a hiatus between the Pabdeh and Sarvak formations. This hiatus encompasses the Gurpi, Ilam, Lafan and even Upper Sarvak formations (Fig. 1c), suggesting a paleo high lineament in the Rag Sefid area (Abdollahie Fard *et al.,* 2006). This lineament is strongly oblique to the Zagros Mountains trend and it affects the axial trends of the overlying folds.

Methods and Materials

Due to the absence surface outcrops of the Asmari reservoir formation in the Rag Sefid Anticline, we used image logs for fracture analysis in this area. Layer boundaries in carbonate sequences are not always sharp and planar due to digenetic processes to be used for structural dip determination (Soleimani *et al.,* 2016). In the FMI and EMI log lines, marking abrupt and relatively high resistivity contrasts that cross all the images is necessary to identify the bed boundaries. These lines are well correlated from pad to pad and are visible on the static images. Their lines correspond to the surface or boundaries separating two beds of different lithology (Serra, 1989). Two types of bedding surface are observed: The first set, in which the dips correspond to sharp and well planar layer boundaries are categorized as High Confidence (HC) whereas in the second set the dips corresponding to vague and uneven bed/layer surfaces are categorized as Low Confidence (LC). We have analyzed the spatial distribution,

orientation, scale and kinematic significance of the fold and fault related fracture systems applying FMI& FMS images log, underground contour map (UGC map), seismic cross-section in the Rockwork software. FMI and EMI log tools can be used in a wide variety of geological and drilling environments providing borehole images of rock from the karstic carbonates to soft thinly laminated sand/shale sequences (Soleimani *et al.,* 2016). Their advantage aspects are high resolution and often complete borehole coverage images. Image log is a pseudo-picture of borehole wall which image the physical property of borehole wall such as electrical resistivity or acoustic impedance (Serra, 1989). In the first method resistivity of borehole wall is converted into high resolution resistivity image of wall. There are 2, 4, 5 or 8 pads on an imaging tool (Fig. 2a). Each pad covers limited part of borehole wall. The FMI tools have an azimuthal resolution of 192◦ capable of radial micro resistivity measurements (vertical resolution: 0.2″, vertical sampling: 0.1″, depth of investigation: 30″) (Ye & Rabiller, 1998). The EMI Electrode arrays are mounted on six independent arms providing excellent pad contact. This produces very high resolution images for stratigraphic and structural analysis. Bedding, fracture features, faults, stratigraphic features and many other characteristics can often be manually or semi-automatically identified and quantified (Ye & Rabiller, 1998). Besides identifying the fractures and faults, borehole imaging logs are routinely used in the support of detailed core analysis for a variety of other applications such as sequence stratigraphy, facies reconstruction and diagenetic analysis (Serra, 1989). In this study, image logs were processed and interpreted by some software such as the CIFLOG GEOMATRIX. When the image is "unrolled" and displayed from 0° to 360°, linear natural features intersecting the borehole appear as sinusoids (Rider, 1996). Assuming that the images are properly oriented to the geographic north, the peaks and troughs of the sinusoids can be related to the dip and azimuth of the associated feature, respectively (Fig. 2b). This consequently provides fundamental information that other petrophysical logs are unable to provide.

Data and results

Structural Dip description

We used image logs in 13 wells in the Rag Sefid anticline to study the fold and fault related fracture systems. For example image logs in the Rag Sefid-G (RS-G) well situated in northeastern flank of the structure are shown for determination geometric features such as bedding and fracture patterns (Fig. 3). With the exception of some short intervals, the entire logged section of the Asmari Formation is layered /bedded as it is comprised of alternating beds/layers of dense and porous limestone of different thickness (Fig. 3).

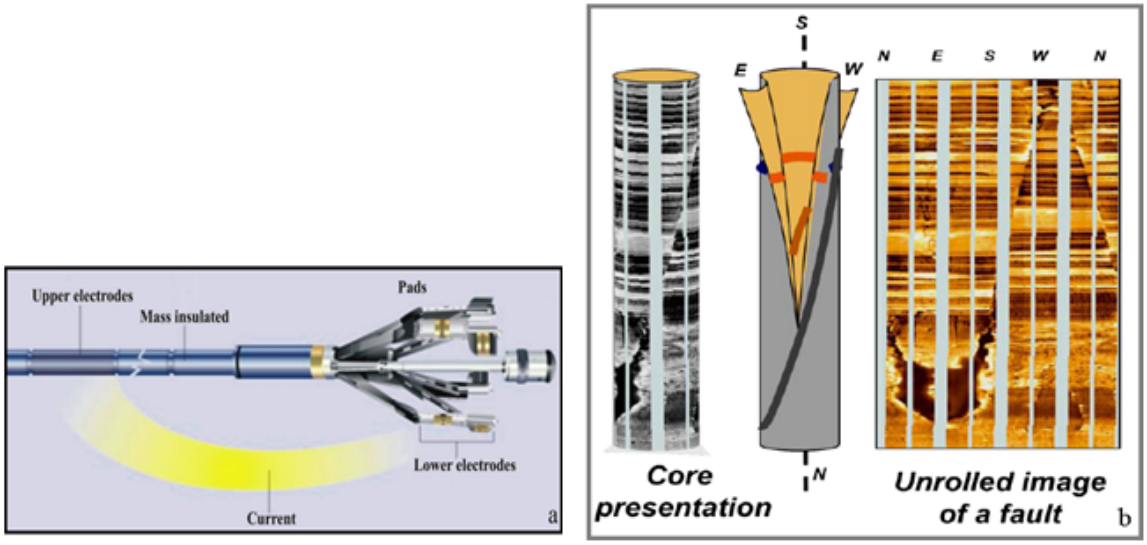

Figure 2. a FMI tool and its pads. Each pad covers limited part of the borehole wall (Soleimani et al. 2016). b Two dimension pictures for calculation of the fracture dip and orientation using image log. Assuming that the images are properly oriented to the geographic north, the peaks and troughs of the sinusoids can be related to the dip and azimuth of the associated feature, respectively (Serra 1989).

Altogether 32 such boundaries were picked out from the FMI images interactively. Most bed/layer boundaries are not so sharp and planar. They generally are uneven due to diagenetic processes. There are 4 bed/layer boundaries which are sharp and planar, hence classified as high confidence for bedding dip and there are 28 less sharp and relatively uneven layer/bed boundaries classified as low confidence bedding. Since the number of high confidence bed boundaries is small, therefore low confidence bedding dips are also considered for structural dip determination. In this well, statistical plots of bedding dips based on 32 readings are presented in Fig. 4, indicating a structural average dip of 22.5 degrees toward N27E and strike N63W-S63E.

Fracture characterization in the RS-G Well

On the FMI and EMI images, fractures tend to occur as linear features that generally have a dip steeper than the structural dip. Open fractures, in a clay free formation, have a conductive appearance on the images due to invasion of their aperture with the conductive drilling mud. The mineralized or sealed fractures appear resistive if the filling material of their apertures is dense like calcite or anhydrite.

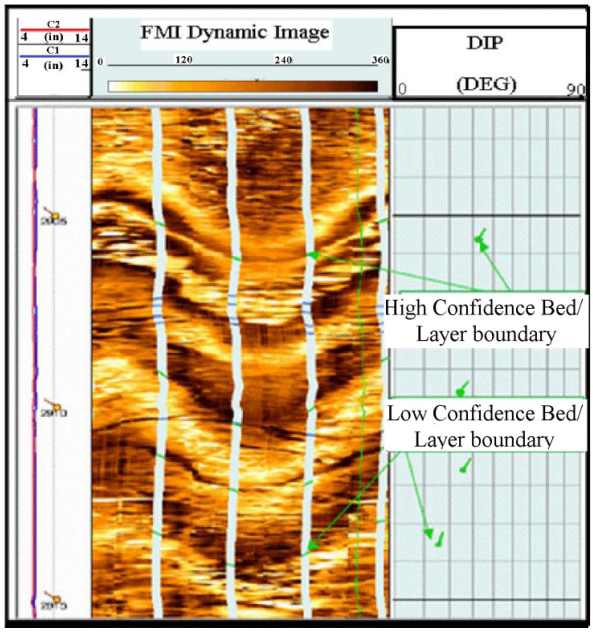

Figure 3. Rather sharp and planar bed boundaries giving high confidence bedding/layering dips in the Asmari Formation of the RS-G well. Low confidence bedding/layering dips corresponding to uneven and less sharp bed/layer boundaries are also indicated

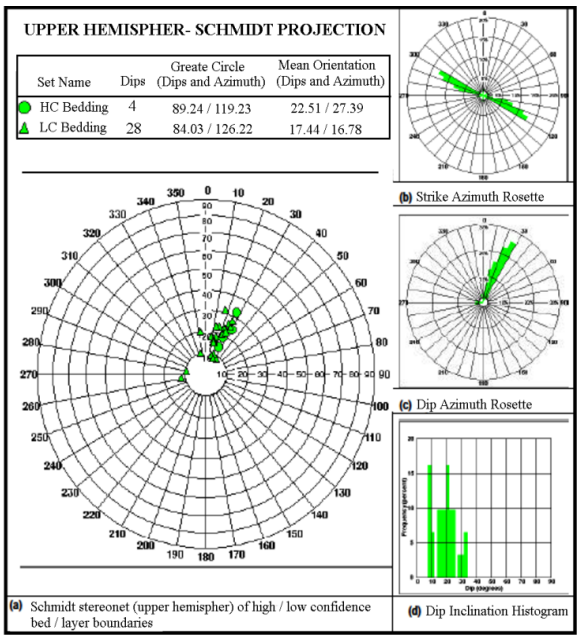

Figure 4. a Shematic stereonet of all high/low confidence bed/layer boundaries found in the Asmari Formation of the RS-G well. b Strike azimuth rosette of bed/layer boundaries. C Dip azimuth rosette of bed/layer boundaries. d Dip inclination histogram of bed/layer boundaries

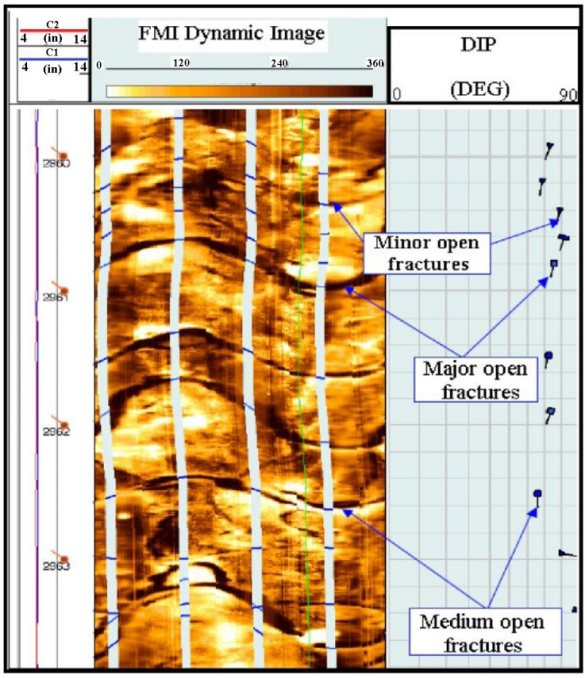

Figure 5. Example of open fractures in Asmari Formation seen by the FMI in the RS-G well

To differentiate between the mud filled and clay/pyrite filled conductive fractures, knowledge of the depositional and stratigraphic setting of the study area is imperative. In some cases, open holes

log can also be very helpful for such kind of differentiation. In the Rag Sefid-G well, the FMI and EMI images revealed a large number of fractures in the Asmari Formation. Altogether 491 fractures were interpreted. Not all fractures have the same appearance as some of them have resistive appearance and some have conductive appearance. This fractures that have continuous or discontinuous conductive traces are termed as open fractures. Their conductive nature is due to mud invasion into the open sections of their planes. Open fractures are further classified into more classes based on their appearance and continuity within the wellbore. Based on observations and interpretation of the images in this well, fracturing is observed throughout the interval (Fig. 5). With the exception of few closed fractures, all 479 fractures are open type. Open fractures strike in one dominant direction, which is N80W and dip dominantly at 67.5 degrees to S10 W (Fig. 6).

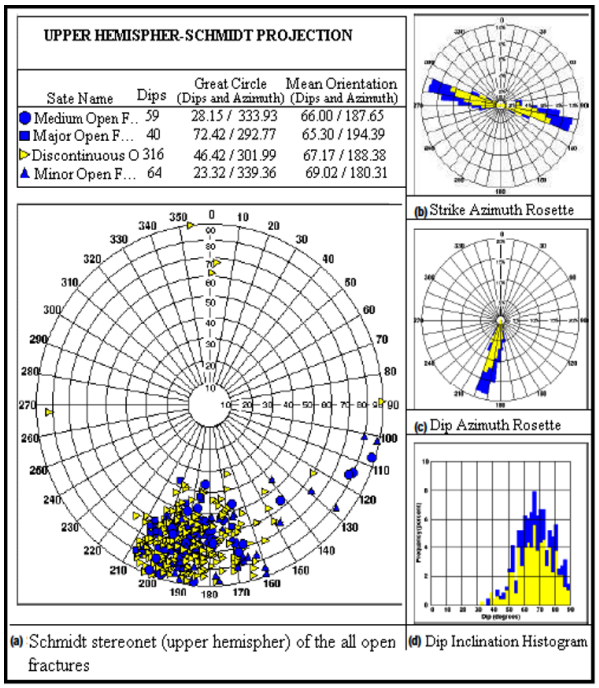

Figure. 6 a Shematic stereonet of all open fractures found in the Asmari Formation of the RS-G well. b Strike azimuth rosette of open fractures. C Dip azimuth rosette of open fractures. d Dip inclination histogram of open fractures

Based on open fracture orientations related to layering, all open fractures in the RS-G Well are divided in three dominant sets. The N35E fracture sets are Cross-axial or transverse fractures, as they strike sub-perpendicular to the axial trace of the anticline. Also the N80W and S40E fractures are longitudinal and oblique sets, as they strike sub-parallel and oblique to the axial trace, respectively.

We identified two structural domains within the Rag Sefid Anticline where the measured linear elements remained homogeneous in their orientation and domains boundary. They have marked by a sharp rotation of fold axial traces. Fractures were assigned to different sets on the stereographic projection. The individual fracture was defined as *axial* and *cross-axial* when the trend of a fracture have measured within the confines of an anticline within 0–10° or 80–90° from the trend of the related fold axial trace , respectively. Fractures trending at higher angles (15°) to the trend of the axial trace were called *oblique* fractures. Two such oblique sets were denoted with the letter *So1* and *So2*. In each of wells, the angular relationships between sets of axial, cross-axial, and oblique fractures were determined. These angles, along with the type of the fracture, were studied in each set for any apparent symmetry and relationship to the axial trace of the confining fold. The bisector angle of the oblique fractures was used to determine the direction of shortening (i.e., the minimum principal stretch, Z axis) for folding and fracturing (Mobasher & Babaie, 2008).

In this study we have analyzed the fractures, i.e., those that occur within the confines of the anticlinal folds and have a geometrical relation to the fold elements, separated from the fault related fractures that occur in the Hendijan-Izeh fault zone and have a systematic angular relationship to the fault.

Discussions

Fold-related fractures

The seismic section of the Rag Sefid Anticline in the Dezful Embayment illustrates the geometry of a typical Dezful Embayment type anticline with poorly imaged forelimb (Fig. 7). However, the gently dipping backlimb and flat-lying hanging wall are an indication of a basement involved structure, which makes this anticline and others like it different to other Zagros anticlines such as typical whale-back anticlines in the Fars region (Sepehr & Cosgrove, 2004).

Based on high aspect ratio (half wavelength to axial length ratio), the Rag Sefid Anticline belongs to the forced folds category (Sattarzadeh *et al.,* 2000). Therefore because of the thrusts development in forelimb and high aspect ratio, the Rag Sefid Anticline is a fault related folding (Sattarzadeh *et al.,* 2000). The axial trace of the Rag

Sefid Anticline is rotated from the regional NW–SE trend to N20° W in the northwest part (Fig. 8). To identify fractures that formed during folding from those that formed due to shearing along the Hendijan-Izeh Fault, we studied fractures in the western part of the Rag Sefid Anticline that include rotated fold and compared them to those immediately outside of the shear zone in the eastern part. Fractures inside and outside of folds can be classified into two general types: intra-fold and trans-fold fractures. An intra-fold fracture is a member of sets of fold-related fractures confined to the interior of fold polygons and also trans-fold fracture, on the other hand, is a member of a sets of fractures that transects (i.e., cuts across) one or more fold polygons.

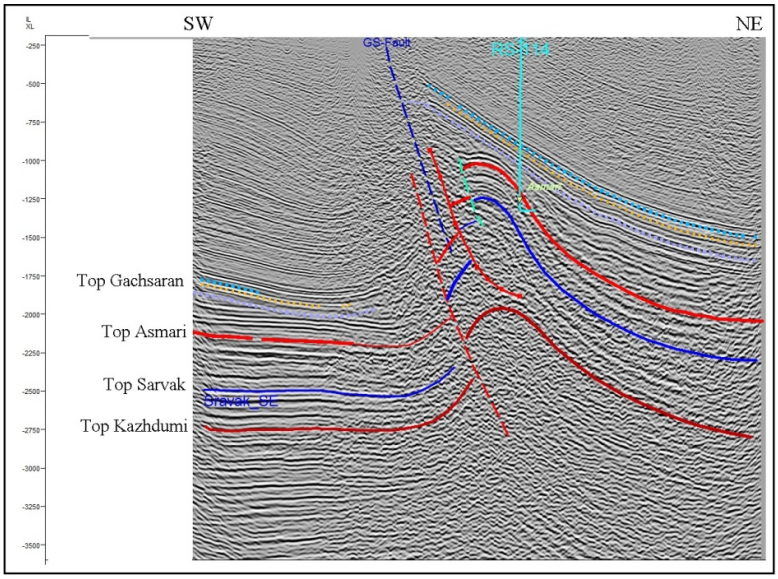

Figure. 7 Seismic reflection profile across the Rag Sefid Anticline. The phenomenon of thrust fault propagation is seen at this Seismic reflection profile

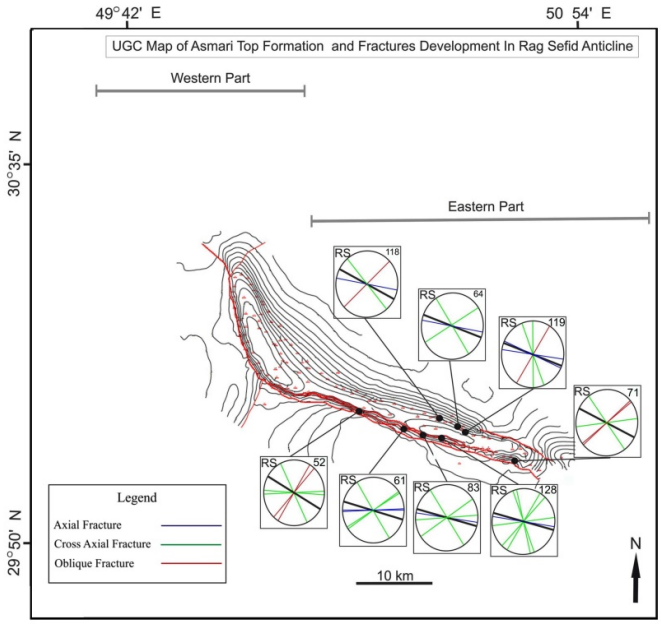

Figure. 8 UGS map from top of the Asmari Formation and illustration of fractures development in the Rag Sefid fold. Note that in the eastern part of fold, strikes of bedding are shown by black lines. Also strikes of axial or longitudinal fractures, cross-axial fractures and oblique fractures are shown by blue, green and red lines respectively. Note the numbers are the well names

The intra-fold fractures suggest a simultaneous formation of the fractures and the confining fold, whereas the trans-fold fractures may be younger than the fold structures (Mobasher & Babaie, 2008). The intra-fold fracture sets have a well-defined geometrical relationship to the restricting fold elements. If the trend of a fracture measured within the confines of an anticline, was within 0–10° or 80–90° from the trend of the related fold axial trace, the individual fracture was defined as *axial* and *cross-axial*, respectively. Fractures trending at higher angles (15°) to the trend of the axial trace were called *oblique* fractures. Two such oblique sets were denoted with the letter *So1* and *So2* (Fig. 8). In this study because we analyzing the open fractures sets by image logs in the 13 wells confined to the interior of fold polygons, this fractures are intra-fold type. For our fold-related fracture analysis, we have selected the eastern part of Rag Sefid Anticline located between 29° 57′ N and 30° 23′ N latitudes, and between 49° 58′ E and 50° 50′ E longitudes. In the Eastern part of the Rag sefid Anticline, images logs of 8 development wells (include RS-52, RS-62, RS-64, RS-71, RS-83, RS-118, RS-119 and RS-128) are available. In each of the wells we interpreted the image logs and detected structural elements such as bedding surfaces (black strikes), axial or longitudinal fractures (blue strikes), cross-axial fractures (red strikes) and oblique fractures (green strikes) shown in Fig. 8.

The traces of the two oblique open fracture sets are oriented N 311°–N 345° and 037°–092°, respectively. In this study, these two sets of shear fractures are referred to as oblique fracture set 1 (SO1) and oblique fracture set 2 (SO2). The mean orientations of the SO1 and SO2 sets are 335±2° and 067±3°, respectively, compared to the 022±2° (i.e., NNE–SSW) mean trend of the cross-axial set. The cross-axial fractures are oriented almost perpendicular to the axial sets and hence, the WNW–ESE trending axial traces of the confining folds. The mean of the two intersecting SO1 and SO2 sets make acute angles (α) of 45±2° and 47±3°, respectively, to the mean cross-axial set (SX) (Fig. 9a). The traces of the two oblique SO1 and SO2 sets are at acute counter clock wise (CCW) and clock wise (CW) angles, respectively, to the fold axial trace. These two sets of oblique fractures may or may not have formed at the same time under the same condition of stress, i.e. they may or may not constitute a conjugate shear fracture set. If they were formed as a conjugate pair, the acute bisector of the two sets would face the direction of the axis of the maximum principal compressive stress (σ1), or instantaneous shortening direction, i.e. the minimum instantaneous stretch (Z-axis) of the strain ellipsoid, assuming a homogeneous deformation (Mobasher & Babaie, 2008). Hence the mean azimuth of the calculated shortening directions for the eastern part of the Rag sefid Anticline is 022°±2. In this paper, since we are dealing with deformed (i.e. folded) rocks, the strain terminology, i.e. maximum stretch direction (Z-axis), is preferred and used instead of the instantaneous stress terms, i.e. the maximum compressive stress (σ1). The results of our fractures analysis of 3992 intra-fold-related open fractures measured in 8 wells in the eastern part of Rag Sefid Anticline are described below and represented in Figs. 9 a.

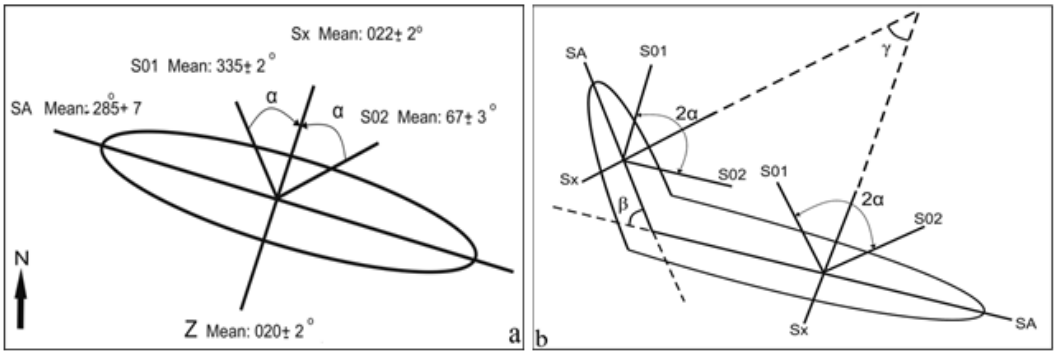

Figure 9. a Schematic illustration of four fracture sets (axial, SA, cross-axial, SX, and the two oblique sets, SO1 and SO2) associated with the Rag Sefid fold. The mean minimum principal stretch axis (Z) (i.e., shortening direction), calculated from these sets of fracture, is assumed to parallel the maximum principal compressive stress (σ). The mean trends of the four fractures sets are also given. The angle α is measured between the cross-axial and the two oblique sets. b Diagram of a fold rotated in the Hendijan-Izeh shear zone. The four fold-related fracture sets (axial, SA, cross-axial, SX, and the two oblique sets, SO1 and SO2) are shown both in rotated and unrotated parts of the Rag Sefid fold. β is the angle of rotation of the Rag Sefid fold axial trace and α is the angle between the cross-axial fracture and the two oblique sets. Also γ is the acute angle between the trend of the SX sets in the both rotated and unrotated parts of the fold

The axial (SA) fracture set has a mean orientation of 285°±7°, which is sub-parallel to 8 wells measured fold axial traces that represent the NW–SE general trend in the Zagros fold belt. The mean orientation of the rotated axial fractures (SA) in the fault zone is 342±2°. The mean trend of the rotated anticlinal axial traces is a function of the orientation of Hendijan-Izeh Fault. In the eastern half of the Hendijan-Izeh Fault zone, the western nose of large anticline that are located in the shear zone, is deformed by the fault operation. To quantify the amount of rotation of the fold in the shear zone, possibly due to faulting, we measured the acute angle (β) between the rotated and unrotated parts of the anticlinal axial traces near the fault (Fig. 9b). The mean rotation angle (β) is 55±4° within the Hendijan-Izeh Fault zone. We also measured the horizontal, acute angle (γ) between the mean trend of the cross-axial set in the rotated and unrotated domain of the deformed fold inside and outside of the shear zone, respectively (Fig. 9b). The mean of the γ rotation angles for the Hendijan-Izeh Fault segment is 44±2°. This rotation angles nearly is close to that indicated by the β angle.

Fault-related fractures

N–S and NE–SW oriented, dextral strike slip faults, such as Hendijan-Izeh, Kazerun, Mengarak, Bala Rud, Korebas, and Sarvestan, intersect the NW–SE and E–W trending Zagros folds. These sub vertical and seismically active faults, which have controlled the Phanerozoic stratigraphy, probably are reactivated basement faults that have been active since the Precambrian (Berberian, 1995; Hessami *et al.,* 2001). All the transverse strike slip faults in the Zagros basement have inherited their roughly north-south strikes from the old grain of Arabia, which can be traced from the central and southern Red Sea (e.g., Schurmann, 1961). These faults are known to be the surface manifestations of the old Pan African structures which have controlled the facies and thickness of sediments deposited since at least the Middle Cretaceous, and which have influenced the styles of their subsequent deformation (McQuillan, 1991). Falcon (1969) first identified the Hendijan-Izeh structure as a lineament on a generalized small scale map; the National Iranian Oil Company then showed it as a north-south trending basement lineament on the tectonic map of SW Iran. The Mountain Front Fault (Fig. 10) is offset right laterally along this strike-slip fault for at least 100 km. If 100 km of right lateral displacement is assumed, this suggests that the Rag Sefid Thrust (RS in Fig. 10) is the dislocated continuation of the Ramhormoz Thrust (RH in Fig. 10). The western end of the Rag Sefid Thrust and the eastern termination of the Ramhormoz thrust suggest drag in the cover associated with a right lateral fault in the basement (Hessami *et al.,* 2001). McQuillan (1991) showed that the edge of the early Jurassic-mid Cretacious Khami shelf, and the edge of the Late Cretacious Sarvak shelf, follows the trend of the Hendijan-Izeh Fault, which must have been active at those times. The Hendijan-Izeh Fault marks the eastern limit of the Dezful Embayment which is bounded in the NW by the left lateral Balarud Fault Zone. The NW end of the Hendijan-Izeh Fault terminates obliquely against the Main Zagros Thrust.

Based on the Basement topography map and Isopach maps illustrating the thickness variation in the Zagros basin between the Fars, Izeh, Dezful embayment, and Lurestan subzones during the Lower–Middle Jurassic and Upper Cretaceous (Abdollahie Fard *et al.,* 2006; Sepehr & Cosgrove, 2004), the Hendijan-Izeh basement fault has N20E trend.

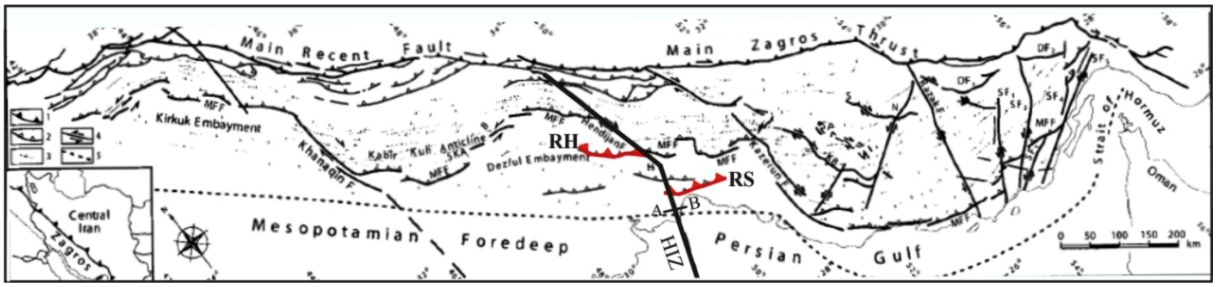

Figure. 10 Structural map of the Zagros fold and thrust belt, showing major faults and anticlinal axes. The abbreviations indicating major structures are as follows: HIF: Hendijan-Izeh Fault, MFF: Mountain Front Fault; B: Balarud Fault Zone; RH: Ramhormoz Fault; RS: Rag Sefid Fault. The western end of the Rag Sefid Thrust and the eastern termination of the Ramhormoz thrust suggest drag in the cover associated with a right lateral fault in the basement (modified from Hessami *et al*., 2001)

A seismic line (AB in Fig.10) that crosses the Hendijan-Izeh high (or Tangu Fault) orthogonally (Fig. 11), shows that thinning of the lower Cretaceous Fahliyan to upper Pliocene Aghajari deposits corresponds to the fault activity and uplift of the Hendijan-Izeh high during the Cretaceous and Tertiary. Thickening of the upper Aghajari represents onset of the Zagros movements which suppress the Hendijan-Izeh high by overload of the upper Aghajari to recent deposits (Abdollahie Fard *et al.,* 2006).

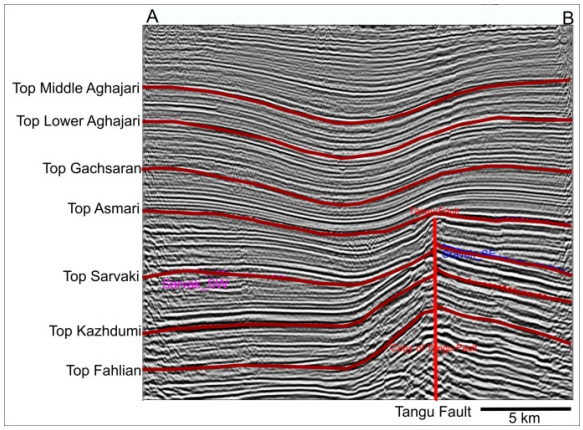

Figure 11. Seismic profile at the top of the Middle Aghajari formation. Note the thickness variations through the Hendijan-Izeh high. Thinning of the lower Cretaceous Fahliyan to upper Pliocene Aghajari deposits corresponds to the fault activity and uplift of the Hendijan-Izeh high during the Cretaceous and Tertiary. Thickening of the upper Aghajari represents onset of the Zagros movements which suppress the Hendijan-Izeh high by overload of the upper Aghajari to recent deposits

Our results show that the N20E trend Hendijan-Izeh right lateral basement fault in the south Dezful Embayment has two parallel segments, caused the restraining bend and dextral shear zone in the western part of the Rag Sefid Anticline. Activity of this shear zone caused clockwise rotation of anticline axis, raising more in the northwest culmination on top of the Asmari Formation than the southeast culmination, form new systems of fracture and also development and increase the density of fractures in the curved part of the Rag Sefid Anticline. We selected an area around the Hendijan-Izeh Fault zone for analysis of the fault related fractures, between 30° 15′ N and 30° 30′ N latitudes and between 49° 45′E and 49° 58′ E longitudes. The NNE–SSW trending Hendijan-Izeh transfer Fault has deformed some of the anticlines through drag and rotation, forming a new system of fractures. The Rag Sefid Anticline is displaced along the Hendijan-Izeh Fault, where the trend of its axial trace has changed from an original N68°W outside of the shear zone, to N20°W in the shear zone. Fault related open fractures are elements of different sets of fractures that form subsidiary to a fault zone to accommodate motion along the main fault. The fault related open fracture sets system includes the following sets: an extensional T-set that may form parallel to the infinitesimal principal shortening direction (Z) and may rotate with continued slip along the fault, synthetic (R) and antithetic (R′) sets of the Riedel shear fracture which form at oblique, acute angles to the horizontal shortening direction, Z (for a vertical, main fault). A synthetic P-shear fracture set may form at a small (< 20°) oblique angle to the main fault. A complete or partial aggregate of these sets of fractures can be used for kinematic purposes to determine the directions of shortening and extension from the fracture orientations. Compared to the R, R′, P and Y-shear fracture, which offset stratigraphic unit boundaries, extensional fractures (i.e., T-set) do not displace contacts (Mobasher & Babaie, 2008). The mean orientation of the Riedel shear (R and R′) in 5 development wells (include RS-67, RS-70, RS-74, RS-111 and RS-136) and the acute angle between them (ρ), are given in Fig. 12 for selected areas of each domain. The mean azimuth of the Riedel R and R′ shear fractures vary across different wells along the fault (Table 1). The mean angle λ between the R Riedel shear fracture and the main shear zone is 19° CW.

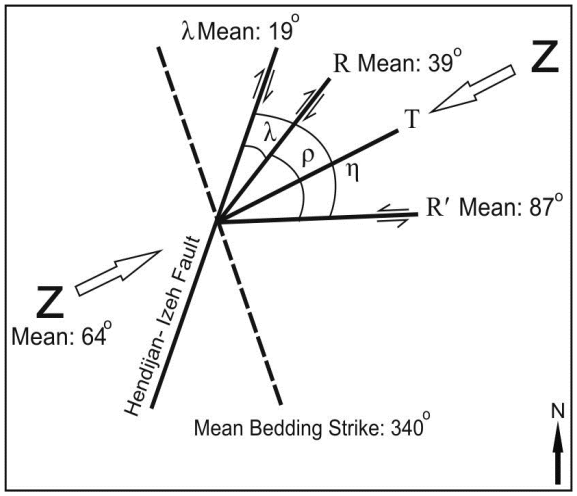

Figure 12. Diagram showing the angular relationships (and their averages) between the right-lateral Hendijan-Izeh fault and the following fault related sets: synthetic Riedel shear fractures (λ); antithetic Riedel shear (η); and synthetic P shear fracture set (φ). Aalso (ρ) is the angle between the two Riedel shear fractures

Table 1. The range of the orientation of the Riedel shears, P-shear and extensional T fractures in western part of the Hendijan-Izeh fault zone

Well Name	R °	R′ °	ρ °	η °	λ°	T°
RS- I	42	89	47	69	22	66
RS- J	32	83	51	61	12	58
RS- K	48	87	40	67	28	68
RS- L	35	86	51	66	15	61
RS- M	35	90	52	70	18	64

The corresponding η angles between the R′ shear fractures and the Hendijan-Izeh Fault are 61–70° CW. The acute angle between the R and R′ fractures (ρ) ranges between 40 and 52° (mean: 45±6°). This angle is bisected by the mean of the extensional fractures (i.e., T set), which is oriented between N58°E and N68° (green strikes in Fig. 13). The P and R shear fracture sets both are synthetic to the right lateral fault zone, and make a low angle from the trace of the fault zone. However, the R shear fractures are more dominant and make a mean angle 19° in CW sense from the Hendijan-Izeh Fault trace, the P-shear sets are less developed in the Hendijan-Izeh shear zone. Also in the western part of the Rag Sefid Fold, longitudinal fractures are developed parallel to bedding strikes (blue strikes in Fig. 13). The mean azimuth of the calculated shortening directions for the western part of the Rag Sefid Anticline is N064°±1 (Figs. 14). The rotation angle for the shortening direction in the eastern part of Rag Sefid Anticline (022°±2) has a range of 42° CW from the shortening direction of the western part of Rag Sefid Anticline (064°±1).

Conclusions

In the Dezful Embayment Fracture sets of the Asmari Formation are created by bending folding due to a protracted contractional process and the new sets of fractures are developed in effect of the reactivation of the basement faults. The contraction was caused by the convergence and ultimate collision of the Arabian and Iranian Plates. We have identified two systems of fractures related to either folding or faulting.

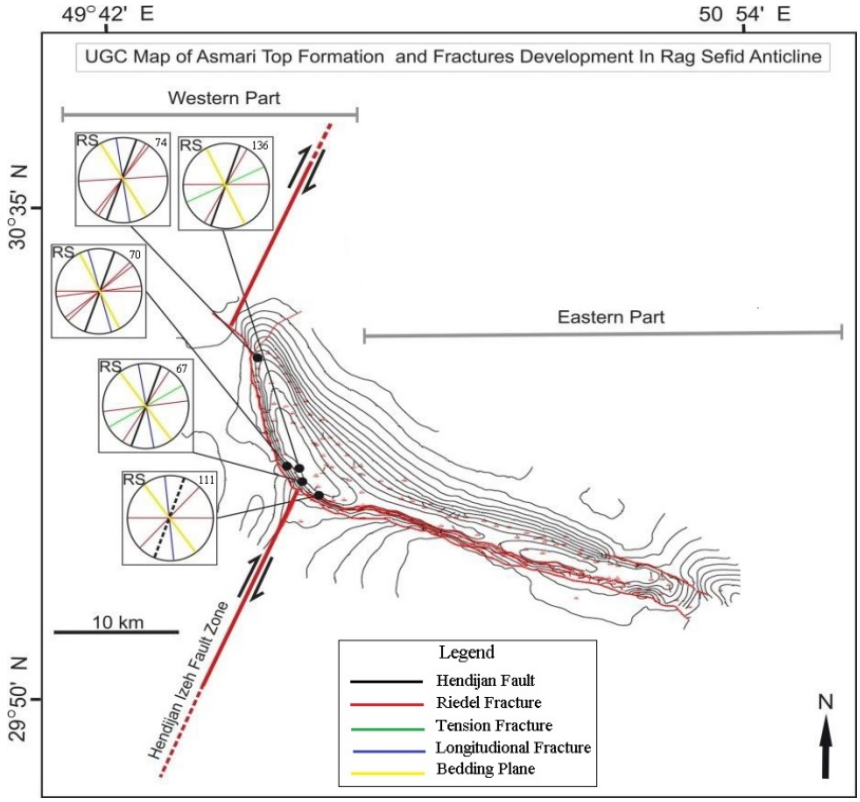

Figure 13. UGS map from top of the Asmari Formation and illustration of fractures development in the western part of the Rag sefid Anticline. Note that in the western part of fold, strikes of the Hendijan-Izeh Fault is shown by black lines. Strikes of Riddle and antithetic Riedel shear fractures are shown by red lines. Also strike of bedding, tensional and longitudinal fractures are shown by yellow, green and blue lines, respectively. Note the numbers are the well names.

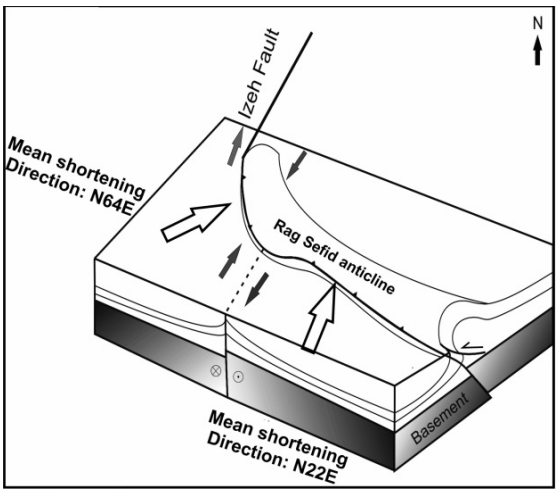

Figure 14. Schematic model of the study area showing the mean azimuth of the shortening directions for the eastern and western part of the Rag Sefid Anticline obtained from fold and fault related fractures. The mean azimuth of the shortening directions is perpendicular to the general trend of the Rag Sefid Anticline in each of the parts.

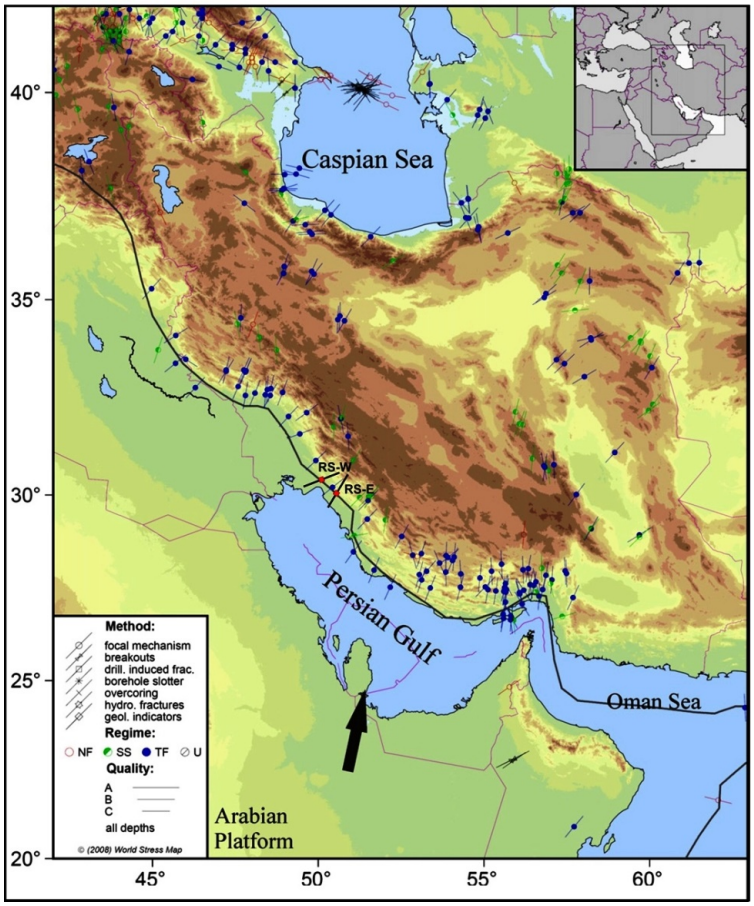

Figure 15. Maximum horizontal stress orientations in Iran from the World Stress Map database and from the wells analyzed herein. Symbols and different colours indicate the method of measurement (circles are focal mechanism solutions, inward facing arrows are breakouts) and the stress regime (NF: normal faulting stress regime; SS: strike slip faulting stress regime; TF: thrust faulting stress regime; black: undefined stress regime). The resultant of the largely NNE and ENE shortening directions observed in the eastern and western wells (RS-E and RS-W) is consistent with S_{Hmax} orientations derived from nearby earthquake focal mechanism solutions observed in the south Dezful embayemen. Heavy arrow shows motion of the Arabian plate relative to the Eurasia (modified from Rajabi *et al.,* 2010)

The fold related system, which includes four sets of fractures, gives shortening orientations consistent with the overall NNE contraction that developed the Zagros folds. The second system of fractures includes three sets formed due to reactivation of the Hendijan-Izeh basement fault. Reactivation of the Hendijan-Izeh basement Faults caused the restraining bend and dextral shear zone in the western part of the Rag Sefid Anticline. Creation of this shear zone caused clockwise rotation of Rag Sefid Anticline axis, change in fractures orientation and also develop and increase the density of fractures in the curved part of Rag Sefid Anticline. The mean shortening (Z-axis) azimuths measured from the fold and fault related fracture systems in the eastern and western part of Rag Sefid Fold are N22±2° and N064±1°, respectively. These shortening directions are perpendicular to the regional trend of the Rag Sefid Anticline axis in each of the parts. Our results show the resultant of the NNE and ENE shortening orientations observed in wells located in the eastern and western parts of the Rag Sefid Anticline is consistent with S_{Hmax} orientations derived from nearby earthquake focal mechanism solutions and with the absolute plate motion direction of the Arabian plate in the Dezful Embayment. We propose that in effect of reactivation of the NNE–SSW oriented dextral strike slip faults such as Hendijan-Izeh Fault, beside the rotation in fold axis, the mean shortening direction in the overall Zagros folds and thrusts belt (NE trend) can be changed and partitioned in two directions in the south Dezful Embayment (Fig. 15).

Acknowledgment

The authors wish to thank National Iranian South Oil Fields Company (NISOC) for sponsorship, data preparation and permission to publish the data. We are grateful to R. Ababafi and M. Yazdani for their cooperation.

References

Abdollahi Fard, I., Braathen, A., Mokhtari, M., Alavi, S.A., 2006. Interaction of the Zagros Fold thrust belt and the Arabian type, deep–seated folds in the Abadan Plain and the Dezful Embayment, SW Iran. Petroleum Geoscience, 12: 347–362.

Agard, P., Omrani, J., Jolivet, L., Mouthereau, F., 2005. Convergence history across Zagros (Iran): constraints from collisional and earlier deformation. Int. J. Earth Sc, 94: 401–419.

Ahmadhadi, F., Daniel, J., Lacombe, O., 2008. Evidence for pre–folding vein development in the Oligo–Miocene Asmari Formation in the Central Zagros Fold Belt, Iran. Tectonics, 27 (TC1016): 1–22.

Bahroudi, A., Koyi, H.A., Talbot, C.J., 2003. Effect of ductile and frictional decollements on style of extension. Jornal of Structural Geology, 25(9): 1401–1423.

Berberian, M., 1995. Master 'blind' thrust faults hidden under the Zagros folds: Active basement tectonics and surface morphotectonics. Tectonophysics, 241(3&4): 193–224.

Beydoun, Z.R., Hughes–Clarke, M.W., Stoneley, R., 1992. Petroleumin the Zagros basin: a Late Tertiary foreland basin overprinted onto the outer edge of a vast hydrocarbon–rich Paleozoic–Mesozoic passive margin shelf. American Association of Petroleum Geologists Bulletin Memoir, 55: 309–339.

Falcon, N.L., 1969. Problems of relationship between surface structures and deep displacements illustrated by the Zagros range, In: Time and place in orogeny. Geol. Soc. London, Spec, 3: 9–22.

Gholipour, A.M., 1998. Patterns and structural positions of productive fractures in the Asmari Reservoirs, Southwest Iran. Journal of Canadian Petroleum Technology, 37: 44–50.

Hessami, K., Koyi, H.A., Talbot, C.J., Tabasi, H., Shabanian, E., 2001. Progressive unconformities within an evolving foreland fold–thrust belt, Zagros Mountains. J. Geol. Soc. London, 158: 969–981.

Inigo, J., Laubach, S., Hooker, J., 2012. Fracture abundance and patterns in the Suband ean fold and thrust belt, Devonian Huama mpampa Formation petroleum reservoirs and outcrops, Argentina and Bolivia. Marine and Petroleum. Geology, 35: 201–218.

Jackson, J.A., McKenzie, D., 1984. Active tectonics of the Alpine–Himalayan Belt between western Turkey and Pakistan. Geophys. J. R. astr. Soc, 77: 185–264.

Lacombe, O., Mouthereau, F., 1999. Qu'est–ce que le front des orogènes? l'exemple de l'orogène pyrénéen. C. R. Acad. Sc, 329: 889–896.

Lacombe, O., Mouthereau, F., 2002. Basement–involved shortening and deep detachment tectonics in forelands of orogens: insights from recent collision belts (Taiwan, western Alps, Pyrenees). Tectonics, 21. doi:10.1029/2001TC901018

Mandl, G., 1988. Mechanics of the Tectonic Faulting, Models and Basic Concepts. Elsevier, London.

Marshak, S., Karlstrom, K., Timmons, J.M., 2000. Inversion of Proterozoic extensional faults: an explanation for the pattern of Laramide and Ancestral Rockies intracratonic deformation, United States. Geology, 28(8): 735–738.

McQuillan, H., 1991. The role of basement tectonics in the control of sedimentary facies, structural patterns and salt plug emplacements in the Zagros fold belt of Southwest Iran. Journal of Southeast Asian Earth Sciences, 5: 453–463.

Mobasher, K., Babaie, H.A., 2008. Kinematic significance of fold– and fault–related fracture systems in the Zagros mountains, southern Iran. Tectonophysics, 451: 156–169.

Mouthereau, F., Deffontaines, B., Lacombe, O., Angelier, J., 2002. Variations along the strike of the Taiwan thrust belt: Basement control on structural style, wedge geometry and kinematics. In Byrne, T.B., Liu, C.S., eds, Geology and Geophysics of an Arc–Continent Collision, Taiwan, Republic of China, Boulder, Colorad. Geol. Soc. Am. Spec. Pap, 358(3) :35–58.

Peska, P., Zoback, M.D., 1995. Compressive and tensile failure of inclined well bores and determination of in situ and rock strength, J. Geophys. Res 100:12791–12811

Pollard, D.D., Aydin, A., 1988. Progress in understanding jointing over the past century. Geological Society of America Bulletin, 100: 1181–1204.

Rajabi, M., Sherkati, Sh., Bohloli, B., Tingay, M., 2010. Subsurface fracture analysis and determination of in–situ stress direction using FMI logs: An example from the Santonian carbonates (Ilam Formation) in the Abadan Plain, Iran. Tectonophysics, 492: 192–200.

Rider, H., 1996. The Geological Interpretation of Well Logs. Gulf Publishing, Texas, 280 pp.

Sattarzadeh, Y., Cosgrove, J.W., Vita–Finzi, C., 2000. The interplay of faulting and folding during the evolution of the Zagros deformation belt, In: Cosgrove, JW, Ameen MS (eds.), Forced folds and fractures. Geol. Soc. London, Spec. Publ, 169: 187–196.

Schurman, H.M.E., 1961. The Riphean of the Red Sea area. Geol. Forch, 83: 109–128.

Sepehr, M., Cosgrove, J.W., 2004. Structural framework of the Zagros foldthrust belt, Iran. Marine and Petroleum Geology, 21: 829–843.

Serra, O., 1989. Formation MicroScanner image interpretation. Schlumberger Educational Services.

Sherkati, S., Letouzey, J., 2004. Variation of structural style and basin evolution in the central Zagros (Izeh Zone and Dezful Embayment, Iran. Mar. Pet. Geol, 21(5): 535–554.

Soleimani, B., Amiri, Kh., Samani, B., Shaban, L., 2016. Lithology effects on the fractures parameters using image log and petrophysical data. Russian Journal of Earth Scince, 16: 1–11.

Talebian, T., Jackson, J., 2002. Offset on the Main Recent Fault of NW Iran and implications for the late Cenozoic tectonics of the Arabia–Eurasia collision zone. Geophys. J. Int, 150: 422–439.

Tapponnier, P., Peltzer, G., Armijo, R., 1986. On the mechanics of the collision between India and Asia. Geol. Soc, Spec. Publ, 19: 115–157.

Vernant, P., Hatzfeld, D., Nilforoushan, F., 2004. Present–day crustal deformation and plate kinematics in the Middle East constrained by GPS measurements in Iran and northern Omam. Geophysical Journal International, 157: 381–398.

Wennberg, O., Svana, T., Azizzadeh, M., Aqrawi, A., Brockbank, P., Lyslo, K., 2006. Fracture intensity vs. mechanical stratigraphy in platform topcarbonates: the Aquitanian of the Asmari Formation, Khaviz Anticline, Zagros, SW Iran. Petroleum Geoscience, 12: 235–245.

Ye, S., Rabiller, P., 1998. Automated fracture detection on high resolution resistivity borehole imagery, SPE annual technical conference and exhibition. Society of Petroleum Engineers, New Orleans, Louisiana, 777–784. https://doi:10.2118/49300–MS

Ziegler, P.A., Cloetingh, S., Van Wees, J.D., 1995. Dynamics of intraplate compressional deformation: the Alpine foreland and other examples. Tectonophysics, 252: 7–59.